DOI: 10.1007/s10297-005-0039-z
Originally published in J. Opt. Fiber. Commun. Rep. 3, 1–24 (2005)

Optical signal processing using nonlinear fibers

Shigeki Watanabe

Fujitsu Laboratories Ltd., Photonics Networking Laboratories (L-50)
4-1-1 Kamikodanaka, Nakahara-ku, Kawasaki 211-8588, Japan
Email: shigeki@labs.fujitsu.com

Abstract. Ultra-fast optical signal processing is a promising technology for future photonic networks. This paper describes possible applications of nonlinear fibers to optical signal processing. The third-order optical nonlinearities in a fiber are discussed by analyzing the interaction of co-propagating optical waves. The properties of a nonlinear fiber are then considered in terms of optimizing the dispersion for achieving phase matching and decreasing walk-off. A highly nonlinear fiber (HNLF) is a practical candidate for an ultra-high-speed signal processor. Using HNLF, the following experiments are successfully demonstated: ultra-broadband wavelength conversion/optical phase conjugation by four-wave mixing, 160 Gb/s optical 3R-regeneration, and optical switching up to 640 Gb/s using a parametric amplified fiber switch. Steps for further improvements are also discussed.

1. Introduction

Optical signal processing is a key technology for making flexible photonic networks. [1] Advanced photonic networks need various kinds of signal processing in optical nodes including optical regeneration, wavelength conversion, optical add-drop multiplexing (OADM) and signal monitoring. [1–35] Fully transparent features in both the time and wavelength domain are required for optical signal processors because the future wavelength-division multiplexed (WDM) networks will utilize ultra-broad bandwidth over 100 nm and the data rate will range from 2.5 to 160 Gb/s or even higher. All-optical signal processors are essential for high-speed networks. Better transparency with ultra-high-speed performance over 160 Gb/s and simultaneous multi-channel processing capabilities clearly distinguish all-optical processors from opto-electronic (O-E) types. [1–11]

An attractive way to realize such transparent optical signal processors is to exploit the third-order nonlinearity in optical fibers. Fiber-based signal processors offer an

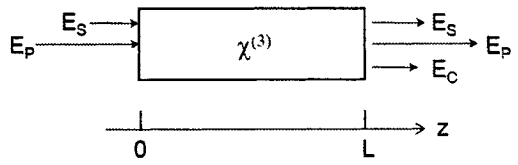

Fig. 1. Generation of optical Kerr-effect in a third-order nonlinear material.

ultra-broad conversion band [3] and ultra-high speed operation at data rates up to Tb/s and above [11] owing to the ultra-fast response time of fiber nonlinearities (several femtoseconds). In order to enable a practical use of fiber-based signal processors, an increase of the nonlinearity coefficient of the fiber and progress in the control of the chromatic dispersion characteristics are necessary. Fibers with high nonlinearity are promising candidates to fulfill the demanding requirements.

This paper describes optical signal processing based on the optical Kerr-effect in nonlinear fibers. Section 2 discusses the third-order optical nonlinearities in a fiber by analyzing the interaction of co-propagating optical waves. Section 3 investigates the properties of a nonlinear fiber for the signal processing in terms of optimizing the chromatic dispersion to achieve the phase matching and to decrease the walk-off among interacting waves. In section 4 a highly nonlinear fiber (HNLF) is shown to be a practical candidate for the ultra-high-speed signal processors. Section 5 reports on examples for the systematic applications. Using the HNLF, ultra-broadband wavelength conversion and optical phase conjugation by four-wave mixing, fiber-based 160 Gb/s optical 3R-regeneration and optical switching up to 640 Gb/s with an optical parametric amplified fiber switch were successfully demonstrated. Steps for further improvements are also discussed in this paper.

2. Third-Order Optical Nonlinearities in a Fiber

Here we analyze the interaction of co-propagating waves in the third-order nonlinear medium with a length L [36]. The schematic configuration is shown in Fig. 1. We consider optical nonlinearities induced by the pump (control) wave E_P with frequency ω_P, assuming the response time of the nonlinear interaction to be faster than the signal pulse duration. Here the "nonlinearities" include self-phase modulation (SPM), cross-phase modulation (XPM) and four-wave-mixing (FWM). E_P interacts with a co-propagating ($+z$ direction) signal wave E_S and an idler wave E_C, where $\omega_P - \omega_C = \omega_S - \omega_P = \delta\omega \neq 0$.

We assume here that we can neglect the wave-vector mismatch. In the slowly varying envelope approximation and supposing all waves to be linearly polarized in the same direction, the differential equations describing the propagation and interaction of these waves are [36,37]

$$\frac{\partial E_P}{\partial z} = \left(-\frac{\alpha}{2} + i\kappa \mid E_P \mid^2\right) E_P \tag{1}$$

$$\frac{\partial E_C}{\partial z} = \left(-\frac{\alpha}{2} + 2i\kappa \mid E_P \mid^2\right) E_C + i\kappa E_P^2 E_S^* \tag{2}$$

$$\frac{\partial E_S^*}{\partial z} = \left(-\frac{\alpha}{2} - 2i\kappa \mid E_P \mid^2\right) E_S^* - i\kappa E_P^{*2} E_C, \tag{3}$$

where α is the loss constant and

$$\kappa = \frac{3\omega\chi^{(3)}}{2nc} \tag{4}$$

denotes the coupling coefficient where $\chi^{(3)}$ denotes the real part of the third-order optical nonlinear susceptibility, ω the optical carrier frequency, n the index of refraction and c the velocity of light. To derive Eqs. (1)–(3), we assumed i) the pump beam depletion is negligible, ii) $\mid E_C \mid^2 \ll \mid E_P \mid^2$ under the initial condition of $E_C(0) = 0$, and iii) the pump power is sufficiently strong where the nonlinearities are essentially due to the pump beam ($\mid E_S \mid^2 \ll \mid E_P \mid^2$). The right-hand terms in Eqs. (1)–(3) describe linear absorption, self and induced optical Kerr effect, and parametric gain by transfer of the two photons from E_P to E_S and E_C. These equations indicate, that induced XPM is twice as effective as SPM; see the factor 2 on the second term of Eqs. (2) and (3). Equation (2) also indicates that the generated idler wave is a complex-conjugate (phase-conjugate) of the signal wave. Following the discussion for these equations [36], first the nonlinear phase shift of E_P is obtained by solving Eq. (1) as

$$E_P(z) = \exp\left(-\frac{\alpha}{2}z\right) \exp[i\phi(z)] E_P(0), \tag{5}$$

where

$$\phi(z) = \kappa \mid E_P(0) \mid^2 \ell(z) \tag{6}$$

is the nonlinear phase shift where $\ell(z) = [1 - \exp(-\alpha z)]/\alpha$ is an effective interaction length. Equations (5)–(6) indicate that the phase of the pump wave changes through propagation in proportion to the power of itself (self-phase modulation).

Substituting Eqs. (5) and (6) in Eqs. (2) and (3), the output waves are obtained under the initial condition of no idler wave input ($E_C(0) = 0$) as

$$E_S(L) = \exp\left(-\frac{\alpha}{2}L\right) \exp[i\phi(L)][1 + i\phi(L)] E_S(0) \tag{7}$$

$$E_C(L) = \exp\left(-\frac{\alpha}{2}L\right) \exp[i\phi(L)][i\phi(L)] E_S^*(0). \tag{8}$$

These equations show parametric amplification with the internal gain factors for E_S and E_C given by

$$G_S = 1 + \phi^2(L) \tag{9}$$

$$G_C = \phi^2(L) = G_S - 1. \tag{10}$$

The conversion efficiencies η_S and η_C are defined by the power ratios of output waves to that of input signal wave ($\eta_S \equiv P_S(L)/P_S(0) = \mid E_S(L) \mid^2 / \mid E_S(0) \mid^2$, $\eta_C \equiv P_C(L)/P_S(0) = \mid E_C(L) \mid^2 / \mid E_S(0) \mid^2$) and are written with use of Eqs. (9) and (10) as

$$\eta_S = \exp(-\alpha L) G_S \tag{11}$$

$$\eta_C = \exp(-\alpha L)(G_S - 1). \tag{12}$$

Equations (6) and (9)–(12) show the parametric amplification process by FWM [36]. Under the condition of using a strong pump wave, where the Kerr-phase shift $\phi(L)$ is sufficiently larger than 1, the power of the signal wave could be increased by the parametric amplification with the gain, which is almost proportional to the square of $\phi(L)$, whereas η_C increases exactly proportional to the square of $\phi(L)$. It is interesting to consider a special model in which XPM only occurs without generating idler wave. If there is no idler wave ($E_C = 0$), the nonlinear phase shift by XPM of E_S is given from Eq. (3) as

$$E_S(L) = \exp\left(-\frac{\alpha}{2}L\right) \exp[i2\phi(L)] E_S(0). \tag{13}$$

As already mentioned, Eqs. (5) and (13) indicate that XPM is twice as effective as SPM as we can see by the factor 2 in the phase term in Eq. (13). The phase shift by XPM can be applied to an optical Kerr-switch.

3. Optical Switching Using Nonlinear Fibers

Signal processing in an optical fiber is based mainly on application of SPM, XPM and FWM. Since these nonlinear optical effects have a response time of several femto seconds, ultra-high-speed and ultra-broadband signal processing is possible.

3.1. Optical Switching by Four-Wave Mixing

Here we discuss signal processing using FWM in fibers. The key issue for applications using fiber-based four-wave mixing is to find condition for increasing the bandwidth.

3.1.1. Phase Matching

To obtain the FWM with sufficiently broad bandwidth, phase matching between interacting waves is required. Considering FWM generated by a signal wave E_S and a pump wave E_P into a dispersion-shifted fiber (DSF) with the length L as depicted in Fig. 1, the phase mismatch, Δk, is approximately written as [3,4,37]

$$\Delta k = \delta\omega^2 \beta_2(\omega_P), \tag{14}$$

where $\beta_2(\omega_P)$ is the second-order dispersion or the group-velocity dispersion (GVD) at the pump frequency ω_P and $\delta\omega$ is a frequency detuning from ω_P. Here we assume that the term of nonlinear phase shift is neglected and the states of polarization (SOP) of the waves E_S and E_P are completely coincided. Equation (14) indicates that the best phase matching ($\Delta k = 0$) is achieved by tuning the pump wavelength λ_P to the average zero-dispersion wavelength λ_0. [3,4,38] However, in an actual fiber, λ_0 usually varies over several nano meters along the line. Fine control of λ_0 is thus indispensable for increasing the conversion bandwidth. The shorter the length of the fiber, the easier it is to control the variance of the dispersion.

Once we achieve the phase-matching, the efficiency of FWM generation is approximately written from Eqs. (6) and (9)–(12) with the input pump power $P_P(0)$ as [3,4]

$$\eta_C(L) = \exp(-\alpha L)[\gamma P_P(0)\ell(L)]^2, \tag{15}$$

where

$$\gamma = \frac{\omega n_2}{cA_{\text{eff}}} \tag{16}$$

denotes the third-order nonlinear coefficient with the nonlinear refractive index n_2 and the effective area of the fiber Aeff.

To obtain a larger η_C, the product $\gamma P_P(0)\ell(L)$ should be increased. It is evident from Eqs. (15) and (16) that the best way to obtain a highly efficient and broadband four-wave mixing in a fiber is to increase γ in order to shorten the necessary fiber length. A highly nonlinear dispersion-shifted fiber (HNLF) is a practical candidate because γ in HNLF increases by germanium doping in the core and by reducing the effective area A_{eff} (mode field area) by a stronger confinement. The HNLF provides highly efficient conversion with a short length, which facilitates control of the λ_0. So far, a HNLF with $\gamma \sim 20\ \text{W}^{-1}\text{km}^{-1}$, which is approximately eight times larger than that of conventional DSF, has been developed. [39]

3.1.2. Bandwidth Increase by Dispersion Arrangement

When we obtain a fiber having a typical bandwidth with some dispersion variance, we can widen the bandwidth by rearranging the dispersion in the fiber [3,5]. In this method, we first measure λ_0 of short sections in which the variance of λ_0 is sufficiently small, then we select sections with similar λ_0 and splice them together. Figure 2 (a) shows the four-wave mixing arrangement using dispersion rearranged 750-m-long HNLF consisting of three 250-m-long sections of HNLF. [5] The 250-m-long sections had the λ_0 values 1547.3, 1546.3 and 1548.4 nm, respectively [see Fig. 2 (b)]. The resultant average λ_0 of the 750-m-long HNLF was 1547.2 nm. The composition of the three sections was arranged such that the first fiber matched with $\lambda_0 = 1547.2$ nm the average zero-dispersion at most while the others were allocated symmetric with this wavelength.

Figure 3 shows the dependence of the conversion efficiency (η_C) versus the signal wavelength measured using the dispersion arranged set-up for four-wave mixing shown in Fig. 2. The 3-dB bandwidth was 34 nm (1530.2–1564.2 nm), which covers almost the entire C-band. The symmetric and flat characteristics show that FWM in HNLF can be applied for wavelength up- and down-conversion of WDM signals.

3.1.3. Ultra-Broad Bandwidth Achieved by a Polarization-Maintained Nonlinear Fiber

For large separation of the wavelengths of the signal wave E_S and the pump wave E_P, polarization-mode dispersion (PMD) appears as a residual limiting factor of the bandwidth. PMD limits the bandwidth because it deteriorates the phase matching between interacting waves. The SOP of the wave transmitted in the fiber depends on the frequency (and so on the wavelength) as [40]

$$\frac{d\mathbf{s}}{d\omega} = \Omega \times \mathbf{s}, \tag{17}$$

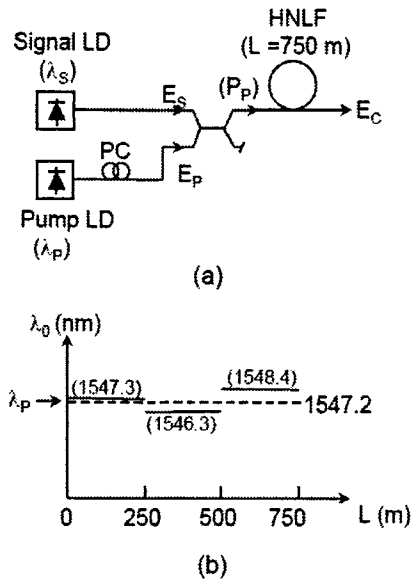

Fig. 2. Four-wave mixing wavelength converter using 750 m HNLF. (a) Configuration, (b) Arrangement of the average zero-dispersion wavelength.

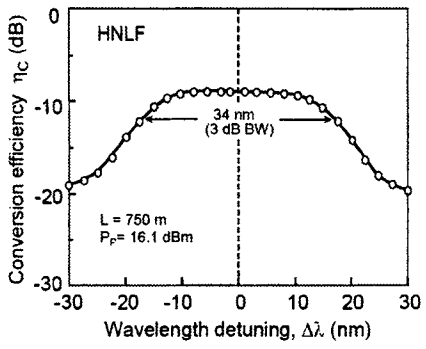

Fig. 3. Dependence of the conversion efficiency, η_C, on the signal wavelength detuning from the pump wavelength, $\Delta\lambda = \lambda_S - \lambda_P$, for a 750-m HNLF four-wave mixer.

where **s** is the unit Stokes vector representing the SOP of the wave and Ω is the rotation vector of the polarization on the Poincare sphere. The rate of rotation of the Stokes vector is equal to the differential group delay time $\delta\tau$ experienced by spectrally narrow pulses having polarizations aligned with the two orthogonal principle states of polarization, [40] i.e.,

$$| \Omega | = | \delta\tau | . \tag{18}$$

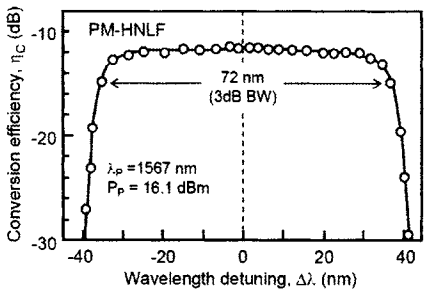

Fig. 4. Conversion efficiency dependence on $\Delta\lambda$ for 1-km PM-HNLF four-wave mixer.

Equations (17) and (18) indicate that the SOP of the largely detuned E_S and E_P change differently in the transmission due to PMD. This severely degrades the phase matching of interacting waves. The bandwidth of FWM, therefore, is limited by the PMD for large detuning condition.

The best way to overcome the PMD problem is the use of a polarization-maintaining (PM) nonlinear fiber.

Figure 4 shows the bandwidth of four-wave mixing using the PM-HNLF. [6] The fiber had a length of 1-km, the third-order nonlinear coefficient of $\sim$11 $W^{-1}km^{-1}$, the zero-dispersion wavelength at 1567.0 nm and a dispersion slope of 0.03 ps/nm^2/km. The crosstalk between the two polarization modes of the fiber was $\sim$25 dB. The 3-dB bandwidth of 72 nm (1532–1604 nm) was obtained with a flattened range of 66 nm. The result clearly shows the bandwidth broadening effect of fixing the SOP in the fiber by reducing the PMD.

3.2. Optical Switching by Cross-Phase Modulation

The phase shift by cross-phase modulation (XPM) in a nonlinear fiber can be applied for optical gating, e.g. in a switch based on a nonlinear optical loop mirror (NOLM) [3,11–13] or in an optical Kerr-switch with XPM-induced polarization rotation. [8,24–26] As shown in Eq. (13) the phase shift by XPM is proportional to the product, $\gamma P_P(0)\ell(L)$, where $P_P(0)$ denotes the input power of a control pulse. A nonlinear fiber with a larger nonlinearity is thus mostly appropriate.

As control pulses become shorter at higher bit rate, the walk-off between the control pulse and the probe light due to group-velocity difference is no longer negligible. The conversion efficiency as well as the speed of switching signal is limited. One way to make the group velocities at both wavelengths the same is to employ a dispersion-flattened fiber (DFF) with a small dispersion. Another way is to utilize specific wavelength allocation using a fiber with dispersion slope.

In a XPM-switch, the walk-off, Δt, between a probe light at a wavelength λ_c and control pulses at λ_s is expressed with the group velocity of the probe light, v_C, and that of control pulses, v_S, as $\Delta t = L[(1/v_C) - (1/v_S)]$, where L denotes the fiber length and group velocities are related with the GVDs as $d(1/v_C)/d\omega = \beta_{2C}$ and $d(1/v_S)/d\omega = \beta_{2S}$. The walk-off is minimized when both group velocities are equal.

Using a DSF with a dispersion slope, walk-off free condition is thus achieved when the wavelengths of the probe light and control pulses are allocated symmetric with respect to λ_0.

In a switching condition in which the phase shift by XPM is π, the effective length $\ell(L)$ is set to

$$\ell(L) = \frac{\pi}{2}\frac{1}{\gamma P_P(0)}. \tag{19}$$

In this equation, it is assumed that the peak power of the control pulses is maintained in the fiber. However, when the required fiber length for the switching condition is longer than the dispersion length, the waveform of the control pulses may be changed by the GVD and SPM. [37] A HNLF with a larger γ is a good candidate for avoiding waveform change since it is effective for shortening the required length L. In addition, a short L is preferable to suppress the walk-off even when the group velocities are not exactly the same.

4. Highly Nonlinear Fibers

From the discussions above it is evident that the best way to obtain a highly efficient and broadband fiber processor is to increase γ, to shorten the necessary length and to achieve fine control of dispersion. Increasing the nonlinearity coefficient reduces the length required to achieve a certain magnitude of nonlinearity, thus enabling more compact devices. Moreover, a shorter fiber length relaxes the requirements regarding the dispersion characteristics, which typically limit the wavelength range of optical signal processing applications. A highly-nonlinear fiber (HNLF) is, therefore, a practical candidate for optical signal processing devices. By germanium doping in the silica-core and reducing the mode field area, a HNLF with $\gamma \sim 20$ $W^{-1}km^{-1}$ has been fabricated. [39] It showed a very good nonlinear feature with finely controlled dispersion profile.

The nonlinearity of fibers can be further increased by reducing the mode field area and by using a core material with a high nonlinear refractive index. Photonic crystal fibers (PCFs) are very promising alternatives to conventional step-index HNLFs. In PCFs, a much stronger confinement of light can be achieved because of the high refractive index contrast between the core and the holey cladding. The majority of highly nonlinear fibers investigated so far are silica-based because of the mature fabrication technology and the low material absorption loss. Nonlinearity coefficients of up to 70 $W^{-1}km^{-1}$ have been reported. [41,42] Other materials such as lead-, [43] chalcogenide-, [44] or Bismuth-oxide-based glasses, [45] however, have a much larger nonlinear refractive index n_2. In a lead glass based PCF, γ-value of 640 $W^{-1}km^{-1}$ has been achieved. [43] An even higher nonlinearity coefficient of 1360 $W^{-1}km^{-1}$ has recently been reported for a Bismuth-oxide-based fiber with a conventional step index design. [45] Decreasing big losses and improving method for a fine control of dispersion are the key issues for these higher nonlinear fibers to be practical.

5. System Applications

Many system applications using the third-order nonlinearities in fiber have so far been demonstrated. Here we show recent results on simultaneous wavelength conversion

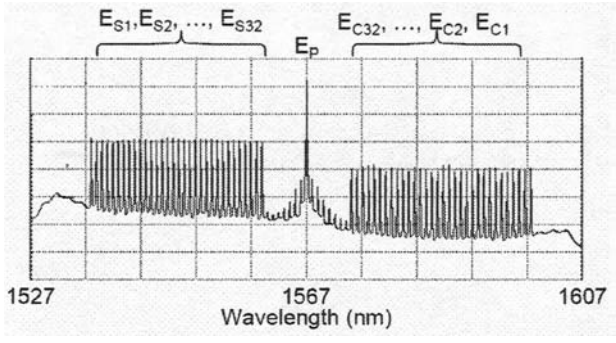

Fig. 5. Optical spectrum of simultaneous conversion of 32 × 10 Gb/s WDM signals output from PM-HNLF four-wave mixer. Res.: 0.2 nm, Vertical scale: 0.2 dB/div.

of WDM signal by FWM, 160 Gb/s optical 3R-regeneration and optical switching up to 640 Gb/s by parametric amplified fiber switch. All of these demonstrations used highly-nonlinear fibers (HNLFs).

5.1. Wavelength Conversion by Four-Wave Mixing

Simultaneous multi-channel wavelength conversion is attractive because it can reduce the number of converters. Using the PM-HNLF four-wave mixer having the bandwidth shown in Fig.4, we performed a simultaneous wavelength conversion of 32×10 Gb/s WDM signal between C-band and L-band. [3,6] The 32 WDM signals E_{Sj} (j=1,...,32) with wavelength at 1535.8 nm (λ_{S1}), 1536.6 nm (λ_{S2}),..., 1560.6 nm (λ_{S32}) (a channel spacing of 100 GHz) were input to the PM-HNLF converter and wavelength converted simultaneously to E_{Cj} at 1599.4 nm (λ_{C1}), 1598.6 nm (λ_{C2}),..., 1573.4 nm (λ_{C32}).

Figure 5 shows the spectrum at the output of the converter. The variance of the conversion efficiency was less than 2 dB for all 32 channels. The FWM crosstalk level between channels were less than −30 dB and no degradation was induced. All channels were converted simultaneously with a power penalty of less than 2.6 dB.

5.2. Optical Phase Conjugation (OPC)

As discussed in section 2, a wave, which is phase-conjugate to the input signal wave, can be generated by FWM [see Eq. (2)]. Using such an optical phase conjugation (OPC) in a transmission link, distortions due to GVD and fiber nonlinearities such as SPM, XPM, FWM and the Raman effect are compensated for. OPC compensates for both positive and negative dispersions and the effects do not depend on the bit rate, pulse shapes and the optical modulation formats. Because of these transparent features OPC has potential to extends flexibility and capacity of future photonic network.

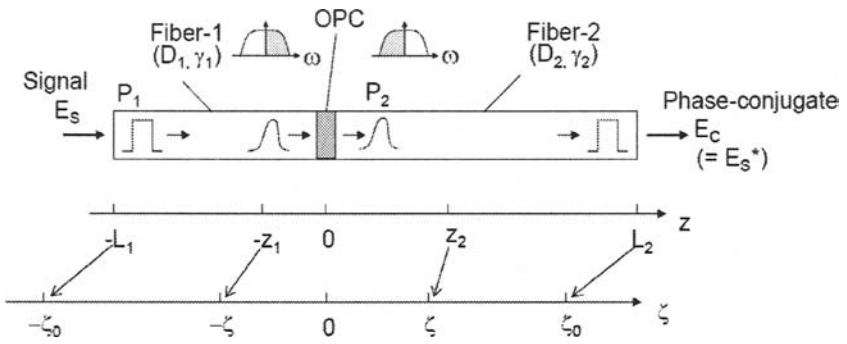

Fig. 6. Schematic configuration of GVD and SPM compensation by OPC. z: actual distance, ζ: normalized distance.

5.2.1. Waveform Distortion Compensation by OPC

Figure 6 illustrates compensation for waveform distortion due to GVD and SPM using optical phase conjugation (OPC). [46] The transmission fiber employs optical amplifiers to compensate for the fiber loss. The signal wave E_S, with optical power P_1 is transmitted through Fiber-1 of length L_1, which has a loss α_1, a dispersion D_1, and an optical nonlinear coefficient γ_1. The optical phase conjugator then converts the wave to a phase-conjugate wave E_C ($\propto E_S^*$) through which the spectrum is inverted with respect to the pump frequency. E_C with optical power P_2 is then transmitted through Fiber-2 with parameters L_2, α_2, D_2 and γ_2. By taking the complex conjugate of the wave, OPC inverts the phase change (modulation) accumulated during transmission over Fiber-1. Waveform distortion is compensated for by giving E_C the same distortion in Fiber-2.

The condition for compensation is approximately achieved when the total GVD in both fibers is identical, [47,48]

$$D_1 L_1 = D_2 L_2, \tag{20}$$

and when the path-averaged SPM-induced phase shift along both fibers is almost the same, [36,46] such that

$$\gamma_1 \overline{P_1} L_1 = \gamma \overline{P_2} L_2. \tag{21}$$

Here, $\overline{P_j} = (1/L_j) \int P_j(z) dz (j = 1, 2)$ indicates the path-averaged power. When SPM can be neglected, as in a transmission with lower signal power level, Eq. (20) is the condition for GVD compensation.

Equations (20) and (21) show the transparent characteristics of OPC, where the compensation conditions do not depend on the modulation format or the bit-rate.

SPM compensation by OPC is limited by the asymmetric distribution of the Kerr-effect along the fiber with respect to the OPC position. This is caused by the asymmetric light intensity change due to fiber loss and amplifier gain. Therefore above approximation applies only when the change of SPM along the fiber is small. An approximate criterion is such that the amplifier spacing is sufficiently shorter than the nonlinear length $L_{\mathrm{NL}} \equiv (\gamma \overline{P})^{-1}$, to keep the optical Kerr phase shift in fiber span small.

A method for the exact compensation of GVD and SPM using OPC has been proposed [46] in which the ratio of dispersion to the strength of the optical Kerr effect is designed to be the same at two corresponding positions, $-z_1$ and z_2, with respect to OPC as follows

$$\frac{D_1(-z_1)}{\gamma_1(-z_1)P_1(-z_1)} = \frac{D_2(z_2)}{\gamma_2(z_2)P_2(z_2)}. \tag{22}$$

Corresponding positions $-z_1$ and z_2 are the points at which the optical Kerr effect or the dispersion (when $D_j(z) \neq 0 (j = 1, 2)$) from the OPC position ($z = 0$) are the same as

$$\zeta = -\int_0^{z_1} \gamma_1(z)P_1(z)dz = \int_0^{z_2} \gamma_2(z)P_2(z)dz \tag{23}$$

or

$$\zeta' = -\int_0^{z_1} D_1(z)dz = \int_0^{z_2} D_2(z)dz. \tag{24}$$

Under the conditions in Eqs. (22) and (23) or Eqs. (22) and (24), the output wave from the second fiber is exactly the complex conjugate of the input wave into the first fiber. The sign of the phase change caused by GVD and SPM at any position $-z_1$, in the fiber is inverted by OPC. Thus the waveform distortion due to above phase shift at position $-z_1$ in the first fiber is exactly compensated for by the distortion due to the phase shift at position z_2 in the second fiber. By providing the equal ratio of the dispersion and the nonlinearity at the corresponding positions throughout the fibers, we can exactly compensate for the waveform distortion due to GVD and SPM. Note that positions $-z_1$ and z_2 are symmetric with respect to OPC if we measure in the normalized distance (see Fig. 6).

The effect of this method was demonstrated in 3000 km transmission system [49] in which the total distortion due to GVD and SPM in a transmission line was given before OPC in the transmitter using dispersion-decreased dispersion compensating fiber.

5.2.2. Simultaneous Compensation of WDM Signals

Using the four-wave mixer with HNLF shown in Figs. 2 and 3, a simultaneous wavelength conversion of 5-channels 40 Gb/s WDM signal were successfully transmitted through 105-km standard fiber using midway OPC. [5] Also using the four-wave mixer with PM-HNLF shown in Fig. 4, 32×10 Gb/s WDM signals were transmitted over a 100-km standard fiber with midway OPC at the 50-km point and additional dispersion compensation at the receiver. [6] Note that only small amount of dispersion compensating fiber (DCF) was required when we used OPC. Since OPC compensates for even-order dispersions (2, 4, ...) and the optical nonlinearities, the spectrum of WDM signals broadened through transmission can be recovered to the original. The simultaneous wavelength conversion and OPC thus can effectively apply for ultra-dense WDM and ultra-high speed transmission in/between future phonic networks.

5.3. Optical 3R Regeneration

An optical 3R-regeneration is an essential technology for optical nodes in future photonic networks. An all-optical 3R-regenerator is especially attractive for high-capacity

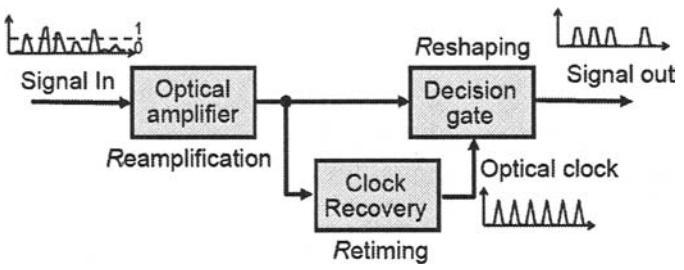

Fig. 7. Basic configuration of an optical 3R-regenerator.

networks, where an opto-electronic (O/E) regenerator will no longer be appropriate. Several methods of all-optical 3R regeneration have been investigated over the last years. [13–26]

Contrary to all-optical 2R-regeneration, e.g., in wavelength converter, in a 3R-regenerator the data signal has to switch a retimed pulse train rather than a continuous wave signal. Therefore, when we apply an optical 3R-regenerator to the 160 Gb/s and higher bit-rate signal, an ultra-high speed and transparent optical gate switch is required. One typical problem of such an ultra-high speed optical switch is that the phase noise or the jitter of the data pulses is converted to the amplitude noise of the output pulses. To overcome this problem, a method was introduced to change the pulse shape of input data signal to a flattened-top shape. [24–26] Another important issue is that the wavelength of the regenerated signal should be the same as that of the input data signal in order to make the design of the transmission link and of switching nodes simple. [25,26]

5.3.1. Optical 3R Regenerator

Figure 7 shows the basic configuration of an all-optical 3R regenerator. Three functions are required for the 3R regenerator: (i) re-amplification, (ii) re-timing and (iii) re-shaping of the input data signal. The operation of re-amplification is basically the same as that of linear amplification.

The re-timing and re-shaping functionalities are achieved in two steps, firstly by synchronizing a train of well shaped optical pulses (optical clock pulses) generated locally by a high-quality pulse source at a repetition frequency corresponding to the line rate of the data signal with the input data signal, and secondly by switching thus generated optical clock pulses in the decision gate by the data signal. For clock recovery, the most popular method is based on converting the optical signal to an electric signal for extracting the clock signal and then on generating the optical clock pulses using a pulse laser. But some electro-optical and all-optical re-timing methods were also proposed. [50–52]

In the decision gate, the data signal switches the locally generated optical clock pulses. For the optical decision gate, a semiconductor-based Mach-Zehnder interferometer, [1,7,18,20] an electro-absorption (EA-) modulator, [21] a nonlinear optical loop mirror (NOLM) [3,13] etc. have so far been proposed. For the operation of the

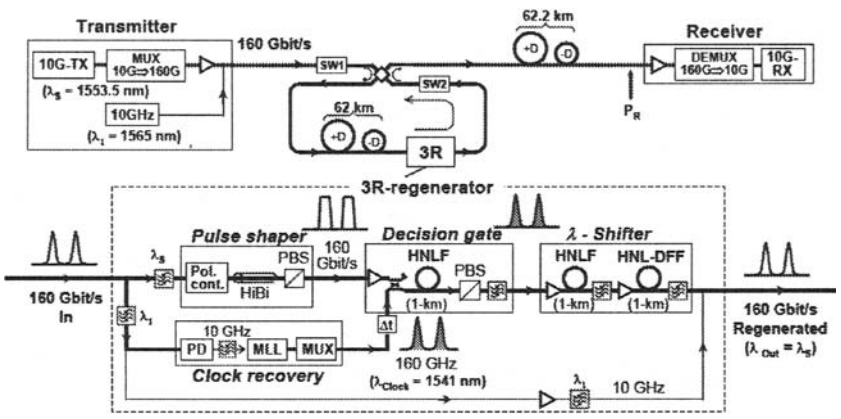

Fig. 8. Experimental setup for 160 Gb/s 3R-regenerating transmission. Inset shows the optical 3R-regenerator.

decision gate it is important that timing fluctuation or jitter of the data signal do not affect the shape of the switched pulses and, more preferably, jitter should be reduced.

Transparent operation is most important for the devices to be applied to optical 3R regenerators. The performance of the regenerator should not depend on the bit-rate, pulse shape and data pattern. The optical nonlinear effects used in the regenerator components should be faster compared with the data rate. If we operate the 3R-regenerator at 160 Gb/s and higher bit rates, the processing speed of the components of the regenerator should be less than 1 pico second. Ultra high-speed optical switches using optical fibers [3,4,11] are candidates for realizing the optical gates. One promising candidate is an optical gate based on cross-phase modulation (XPM) in an optical fiber. [24–26]

5.3.2. 160 Gb/s Optical 3R Regeneration Experiment

Figure 8 shows the setup for the 160 Gb/s 3R-regenerating transmission in a circulating loop comprising a 62-km long fiber span and the optical 3R-regenerator. [25,26] In the transmitter, a mode-locked laser generated a 10-GHz optical pulse train ($\sim$1.6 ps FWHM) at λ_s = 1553.5 nm, which was modulated by a $LiNbO_3$ intensity modulator (10 Gb/s, PRBS: $2^{23} - 1$) and optically time-division multiplexed (OTDM) to a 160-Gb/s single-polarization data signal. In the receiver, the 160-Gb/s data signal was demultiplexed to a10-Gb/s signal and detected.

The inset in Fig. 8 shows the configuration of the 160-Gb/s optical 3R-regenerator. It comprised four distinct elements: the pulse shaper, the decision gate, the optical clock recovery and the wavelength shifter.

The pulse shaper shapes input pulses into flattened-top ones using a piece of highly birefringent fiber (HiBi-fiber) and the polarization beam splitter. As shown in Fig. 9 the pulse shaper generated pulses having a well-flattened top (FWHM $\sim$2.7 ps) and with leading and trailing edges as given by the input pulses. An optical Kerr-switch utilizing XPM induced polarization rotation in a HNLF ($\gamma = 20\ W^{-1}km^{-1}$) functioned as

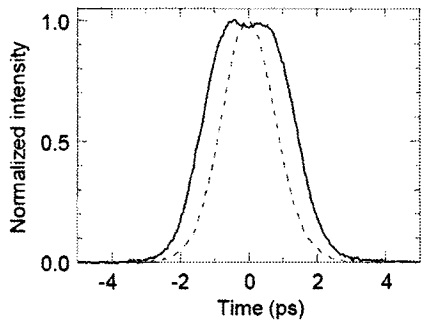

Fig. 9. Cross-correlation traces measured with a 650-fs $sech^2$ pulse (- - - input, — output signal of the pulse shaper).

decision gate, in which the 160-Gb/s flattened-top signals switched the locally retimed 160-GHz optical clock pulses. Owing to the pulse shaper, the decision gate was less sensitive to the jitter of the incoming data pulses (more than four times enlargement of the phase margin) and effectively suppressed the jitter as well as the amplitude noise. At the output end of the decision gate, the wavelength shifter reset the wavelength of the regenerated signal to that of the input data signal. A fiber-based wavelength shifter was employed, which broadened the signal spectrum followed by optical filtering. A regenerator with no wavelength shift is advantageous to make the design of the transmission link (dispersion compensation) and of switching nodes simpler. Note that the wavelength shift using spectrum broadening can further improve the performance of the regenerator by its 2R-regeneration effect. [53]

Figure 10 shows the power penalties (at BER = 10^{-9}) for all the 16 OTDM channels with and without 3R-regenerator measured at 62, 124 and 186 km. Compared with the results without the 3R-regenerator, 3R-regenerator well improved system performance with suppressing noise of the signal, and 160-Gbit/s optical 3R-regenerating transmission in a circulating loop was successfully demonstrated. The results indicate that the quality as well as the wavelength of the regenerated signal is almost the same as that of the original signal, which is an essential prerequisite of the 3R-regenerator.

5.4. Optical Parametric Amplified Fiber Switch

An ultra-high speed optical switch is one of the key devices for optical signal processing. [1] For practical applications, the switch should operate with high efficiency, be fully transparent in the data rate and in a wavelength range covering at least one band, e.g., the whole C or L-band. For applications such as optical add-drop multiplexing or optical 3R-regeneration, the input and output wavelengths should be same.

This section shows a fiber based optical switch operating in a full transmission band without wavelength shift and having a very high S/N ratio because it provides parametric gain. [54] Contrary to switching devices based solely on parametric gain, [55] the switch has also a very high contrast ratio. Its good and stable performance is shown in 160, 320, and 640 Gb/s optical demultiplexing and optical sampling experiments.

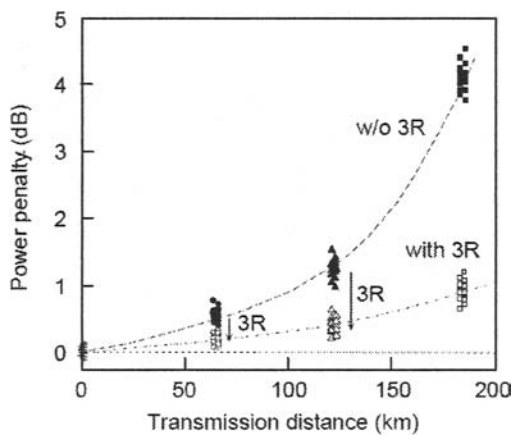

Fig. 10. Power penalty at BER = 10^{-9} versus transmission distance measured at 62, 124, and 184 km points with and without optical 3R-regeneration.

5.4.1. Principle and Operation of the Switch

The scheme of the optical switch is shown in Fig. 11. [54] The optical signal E_S (data pulses, wavelength λ_S and pulse peak power P_S) and control (pump) pulses E_P (λ_P, P_P) are input to a highly-nonlinear fiber (HNLF). Behind the HNLF is a polarizer, which transmits only light linearly polarized along the main axis of the polarizer (vertical axis in Fig. 11). Using a polarization controller, the state of polarization of E_S at the input of the HNLF is set linear and orthogonal (in the absence of a control pulse) to the main axis of the polarizer, so that no light is transmitted. The state of polarization of E_P is aligned at $\sim$45. E_P causes a change of the state of polarization of E_S by FWM and therefore transmission of the data signal with increasing P_P. The distinguished feature of the proposed switch is that it uses optical parametric amplification by FWM. The parametric amplification of the polarization component of E_S along E_P leads to an amplification of E_S and an additional change of the state of polarization. The polarization of E_S clamps at a linear polarization state with an angle θ near $\sim$45°, even if P_P is further increased.

This switch does not shift the wavelength of the signal. It has a good extinction ratio of more than 30 dB, and the switched pulses have a very high optical S/N ratio because they are parametrically amplified. Note that the peak power P_S of the output signal is increased even if we count the 3-dB loss added by the polarizer in the condition of θ $\sim$45°. Considering the ultra-fast response time of FWM of several femto seconds, the proposed switch can be applied to ultra-high speed (>Tb/s) signal processing.

5.4.2. Ultra-Broadband and Highly Efficient Switching

The switch was tested using a 20-m-long HNLF with $\gamma = 20.4\ \mathrm{W^{-1}km^{-1}}$, $\lambda_0 \sim 1579$ nm and a dispersion slope of 0.03 ps/nm^2/km. [3] Figure 12 shows the experimental setup. [54] A mode-locked fiber laser (MLFL1) generated a 10-GHz optical pulse train

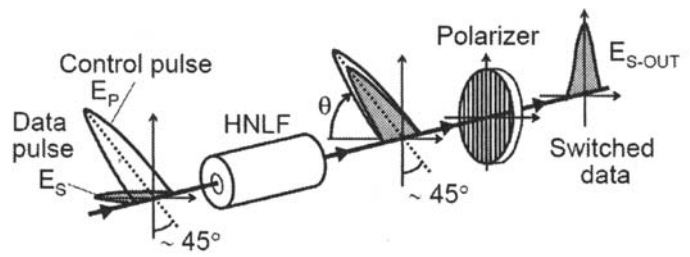

Fig. 11. Schematic of optical parametric amplified fiber switch.

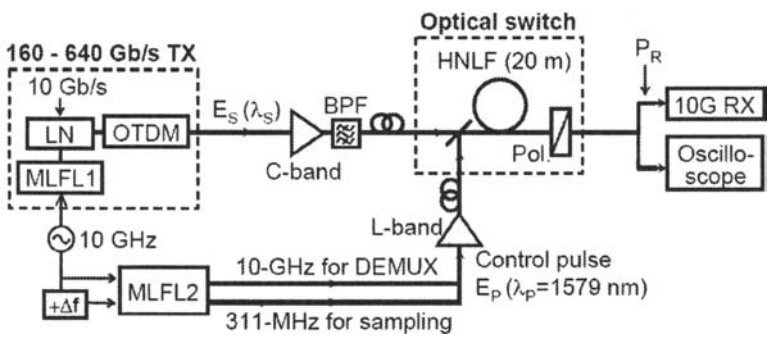

Fig. 12. Experimental setup for optical parametric amplified fiber switch.

at the wavelength λ_S in the C-band, which was modulated at 10 Gb/s (PRBS: $2^{23}-1$) and then OTDM-multiplexed to a single polarization 160–640 Gb/s data signal E_S. E_S was input to the HNLF together with the control pulses E_P generated by the second MLFL2. E_P had a wavelength located at the L-band ($\sim \lambda_0$) and $\sim$45°-aligned polarization.

Figure 13 shows the switching gain versus the control peak power P_P of 10 GHz control pulse at λ_S = 1550 nm. The pulse widths (FWHM) of E_S and E_P were 1.6 and 0.9 ps, respectively. Here the switching gain is defined as the ratio of P_S at the output of the polarizer to P_S at the input of the HNLF. Since dominant parametric gain was given in parallel polarization condition for both pulses, the output power of E_S increased proportional to P_P^2 by optical parametric amplification as discussed in section 2. The highest switching gain of 7.6 dB at $P_P \sim 15$ W (averaged power of $\sim$+21 dBm for used 10 GHz pulses) was obtained with 20-m HNLF. Figure 14 shows the switching gain versus the wavelength of E_S at P_P 15 W confirming almost flat gain over the full C-band owing to a good phase-matching and small walk-off in 20-m HNLF. Note that by allocating the wavelength of E_P in the C-band, we can provide an optical switch operating over the full L-band.

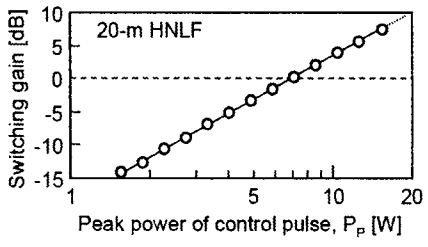

Fig. 13. Switching gain dependence on the control power.

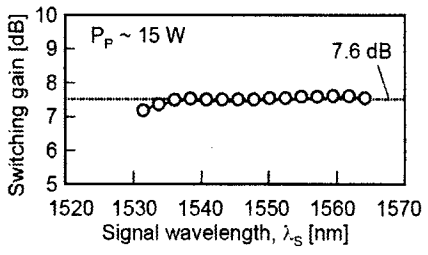

Fig. 14. Switching gain dependence on the signal wavelength.

5.4.3. Ultra-High-Speed Switching Demonstration

Using the optical fiber switch above, we performed optical demultiplexing experiments of 160, 320 and 640 Gb/s OTDM signals E_S to 10 Gb/s. [54] The pulse width of E_S was 1.6 ps for 160 Gb/s, 0.75 ps for 320 Gb/s and 0.65 ps for 640 Gb/s, whereas that of E_P was fixed at 0.9 ps. Figure 15 shows BER measurements versus the received power P_R of the demultiplexed signal at an average control power of +21.8 dBm (corresponding to $P_P \sim 15$ W). For 160 Gb/s, we measured BERs at signal wavelengths of $\lambda_S = 1535$, 1540, 1550 and 1560 nm.

Error free operation with power penalties (at BER = 10^{-9}, compared to the 10-Gb/s reference) of less than 0.2 dB was achieved for all wavelengths, demonstrating operation of this switch in the full C-band. We confirmed the error free operation at the input powers larger than -5 dBm of the 160-Gb/s signal. Error free operation was also achieved for 320 and 640 Gb/s signals with a slight increase of the power penalty of 1.1 and 2.5 dB, respectively, mainly caused by a residual cross-talk due to insufficiently short pulse widths.

5.5. Optical Sampling

Monitoring the quality of ultra-short pulses is an important issue in high-speed networks. Electrical sampling systems are commonly used to observe optical signals using O-E conversion. However, the bandwidth determined by the operation speed of the electronics is so far limited up to ~100 GHz at most. By using the ultra short pulse

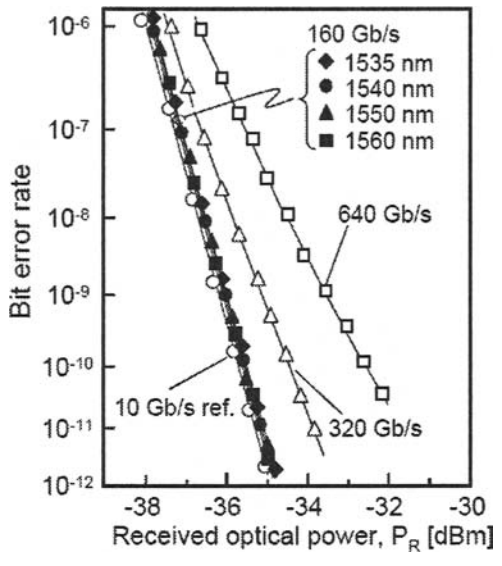

Fig. 15. Bit-error rate characteristics for the demultiplexed 10 Gb/s signal from 160, 320 and 640 Gb/s OTDM signal.

technology, optical sampling enables the direct observation of the waveform of 160 Gb/s and higher bit-rate signals. [30–35] A fiber-based optical gate is attractive for optical sampling. [30–31] because it offers higher conversion efficiency compared to optical gates based on nonlinear crystals and it also provides less than pico second time resolution.

Using the parametric amplified fiber switch described in the former section, a 160–640 Gb/s optical sampling system was demonstrated [54] using an all-optical clock recovery based on an optical phase locked loop (PLL). Figures 16 (a)–(e) show the eye-patterns observed with the same pulse widths as used in the BER measurements shown in Fig. 15. With an excellent high contrast and ultra-fast response provided by the fiber switch, clear eye-patterns of 160–640 Gb/s data were monitored with an excellent time resolution. The results indicate the possibility of optical sampling with high contrast and coverage of the entire C-band.

5.6. Supercontinuum Generation

Supercontinuum (SC) light can be generated using nonlinear fibers. [27–29] An impressive example of SC generation is the realization of a multi-wavelength source with more than 1000 channels. [27] SC with high spectral density is highly desirable for practical reasons. It can be achieved in the normal dispersion regime of fibers where chirping by self-phase modulation (SPM) is accumulated. When a part of the generated SC is filtered out with an optical filter, wavelength conversion is realized. Using a

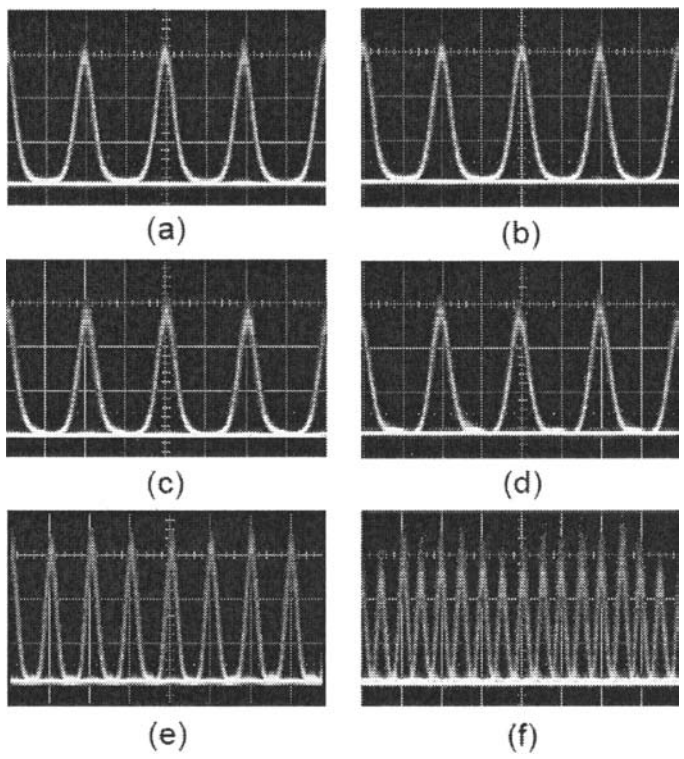

Fig. 16. Eye patterns of OTDM signal monitored by the optical sampling oscilloscope configuration using the optical parametric amplified fiber switch as a sampling gate. 160 Gb/s signal at (a) 1535 nm, (b) 1540 nm, (c) 1550 nm and (d) 1560 nm; (e) 320 Gb/s at 1550 nm and (f) 640 Gb/s at 1550 nm. Sampling rate: 311 MHz; Horizontal scale: 3.125 ps/div.

dispersion-flattened fiber with normal dispersion for SC generation, wavelength conversion at 160 Gb/s was demonstrated. [25,26,56] SC also provides a 2R regeneration function, which improves the quality of the signal. [53] This 2R effect was confirmed in a 160-Gbit/s regenerating conversion node. [57]

6. Summary

The effectiveness of nonlinear fibers for all-optical signal processing and the potential applications were described. The highly-nonlinear fiber (HNLF) is presently the most practical fiber so far developed and applied to optical signal processing. Various systematic applications have so far been demonstrated using HNLFs. Most of these demonstrations showed unique and attractive features which could not achieved without using the third-order optical nonlinearity in fiber.

By using four-wave mixing, WDM signals over almost entire C-band were simultaneously wavelength-converted to L-band. Fine control of a chromatic dispersion

as well as polarization-mode dispersion is essential to realize sufficiently broadband wavelength converter. Optical phase conjugation was also applied to WDM signal and well compensated for waveform distortion of all the channels simultaneously. The configuration and operation of an optical 3R regenerator, especially for 160 Gb/s data transmission, were described. One critical issue of using an ultra-fast optical gate switch is the conversion of timing jitter in the incoming data signal to amplitude noise in the output data signal. By using a pulse shaper at the input of the optical Kerr-switch used as a decision gate, we successfully reduced this detrimental effect and demonstrated 160 Gb/s optical 3R-regenerating transmission. Finally, an optical parametric amplified fiber switch was shown. The switch operated in a full transmission band without wavelength shift and having a very high S/N ratio and contrast ratio because it provides optical parametric gain. Using a 20-m-long highly-nonlinear fiber, optical demultiplexing and optical sampling of up to 640 Gb/s signals were successfully demonstrated over the whole C-band by using a fixed control pulse located in the L-band.

The ultra-broadband and ultra-high speed features of fiber-based optical signal processors enable us to realize Tb/s order optical switching in future photonic networks. Further increase in the nonlinearity is the key issue in realizing breakthrough fiber-based optical signal processors. Rapid development in nano-optical devices such as photonic crystal fibers, holey fibers and quantum dot amplifiers [58] is thus being demanded.

Acknowledgment

The author acknowledges F. Futami, S. Takeda, and R. Okabe at Fujitsu Laboratories Ltd. for their useful discussion and contribution in the systematic demonstrations, H.G. Weber, R. Ludwig and their colleagues at the Heinrigh-Hertz Institut (HHI) for their collaboration and useful discussion, and Sumitomo Electric Industries for producing highly-nonlinear fibers.

References

1. K.E. Stubkjaer, Semiconductor optical amplifier-based all-optical gates for high-speed optical processing, IEEE J. Select Top Quantum Electron, **6**, 1428–1435 (2000).
2. S.J.B. Yoo, Wavelength conversion technologies for WDM network applications, J. Lightwave Technol., **14**, 955–966 (1996).
3. S. Watanabe and F. Futami, All-optical signal processing using highly-nonlinear optical fibers, IEICE Trans., **E84-B**, 1179–1189 (2001).
4. S. Watanabe and F. Futami, All-optical wavelength conversion using ultra-fast nonlinearities in optical fiber, IEICE Trans., **E85-C**, 889–895 (2002).
5. S. Watanabe, S. Takeda, G. Ishikawa, H. Ooi, J.G. Nielsen, and C. Sonne, Simultaneous wavelength conversion and optical phase conjugation of 200 Gb/s (5×40 Gb/s) WDM signal using a highly nonlinear fiber four-wave mixer, Proc. Integrated Optics and Optical Fiber Communications/24th European Conference on Optical Communications (IOOC/ECOC'97) at Edinburgh, UK, September 1997, Post-deadline Paper TH3A, pp.1–4.

6. S. Watanabe, S. Takeda, and T. Chikama, Interband wavelength conversion of 320 Gb/s (32×10 Gb/s) WDM signal using a polarization-insensitive fiber four-wave mixer, Proc. 24th European Conference on Optical Communications (ECOC'98) at Madrid, Spain, September 1998, Post-deadline paper, p. 85.
7. S. Nakamura, Y. Ueno, and K. Tajima, 168-Gb/s all-optical wavelength conversion with a symmetric-Mach-Zehnder-type switch, Photon. Technol. Lett., **13**, 1091–1093 (2001).
8. J. Yu and P. Jeppesen, 80-Gb/s wavelength conversion based on cross-phase modulation in high-nonlinearity dispersion-shifted fiber and optical filtering, IEEE Photon. Tech. Lett., **13**, 833–835 (2001).
9. U. Feiste, R. Ludwig, C. Schubert, J. Berger, C. Schmidt, H.G. Weber, B. Schmauss, A. Munk, B. Buchold, D. Briggmann, F. Kueppers, and F. Rumpf: 160 Gbit/s transmission over 116 km field-installed fiber using 160 Gbit/s OTDM and 40 Gbit/s ETDM, Electron. Lett., **37**, 443–445 (2001).
10. S. Kawanishi, H. Takara, K. Uchiyama, I. Shake, K. Mori, 3 Tbit/s (160 Gbit/s x 19 channel) optical TDM and WDM transmission experiment, Electron. Lett., **35**, 826–827 (1999).
11. M. Nakazawa, T. Yamamoto, and K. R. Tamura, 1.28 Tbit/s-70 km OTDM transmission using third- and fourth-order simultaneous dispersion compensation with a phase modulator, Electron. Lett., **36**, 2027–2029 (2000).
12. M. Jinno, Effects of group velocity dispersion on self/cross phase modulation in a nonlinear Sagnac interferometer switch, J. Lightwave Technol., **10**, 1167–1178 (1992).
13. J.K. Lucek and K. Smith, All-optical signal regenerator, Opt. Lett., **18**, 1226–1228 (1993).
14. J.C. Simon, L. Billes, A. Dupas, and L. Bramerie, All optical regeneration techniques, Proc. 25th European Conference on Optical Communication (ECOC'99) at Nice, France, 1999, II, pp. 256–257.
15. B. Sartorius, All-optical 3R signal regeneration, Proc. 26th European Conference on Optical Communication (ECOC2000) at Munich, Germany, September 2000, Paper 9.4.1, pp. 293–294.
16. H. Yokoyama, H. Kurita, T. Shimizu, I. Ogura, Y. Hashimoto, R. Kuribayashi, M. Shirane, and H. Yamada, All-optical clock extraction and signal regeneration with mode-locked laser diodes, Proc. 7th International Workshop on Femtosecond Technology (FST 2000) at Tukuba, Japan, June 30, 2000, p. 71.
17. B. Sartorius, C. Bornholdt, S. Bauer, M. Moehrle, P. Brindel, and O. Leclerc, System application of 40 GHz all-optical clock in a 40 Gbit/s optical 3R regenerator, Proc. Optical Fiber Communication Conference (OFC 2000) at Baltimore, USA, 2000, Paper PD11.
18. D. Wolfson, A. Kloch, T. Fjelde, C. Janz, B. Dagens, and M. Renaud, 40-Gb/s all-optical wavelength conversion, regeneration, and demultiplexing in a SOA-based all-active Mach-Zehnder interferometer, IEEE Photon. Technol. Lett., **12**, 332–334 (2000).
19. A.E. Kelly, I.D. Phillips, R.J. Manning, A.D. Ellis, D. Nesset, D.G. Moodie, and R. Kashyap, 80 Gbit/s all-optical regenerative wavelength conversion using semiconductor optical amplifier based interferometer, Electron. Lett., **35**, 1477–1478 (1999).
20. Y. Ueno, S. Nakamura, and K. Tajima, Penalty-free error-free all-optical data pulse regeneration at 84 Gbps with Symmetric-Mach-Zehnder-type regenerator, Proc. Optical Fiber Communication Conference (OFC 2001) at Anaheim, CA, USA, 2001, Paper MG5-1.
21. T. Otani, T. Miyazaki, and S. Yamamoto, Optical 3R regenerator using wavelength converters based on electroabsorption modulator for all-optical network applications, IEEE Photon. Technol. Lett., **12**, 431–433 (2000).

22. M. Nakazawa, E. Yamada, H. Kubota, and K. Suzuki, 10 Gbit/s soliton data transmission over million kilometers, Electron. Lett., **27**, 1270–1272 (1991).

23. S. Bigo, O. Leclerc, and E. Desurvire, All-optical fiber signal processing and regeneration for Soliton communications, IEEE J. Select. Top. Quantum Electron., **3**, 1208–1223 (1997).

24. R. Ludwig, C. Schubert, S. Watanabe, F. Futami, C. Schmidt, J. Berger, C. Boerner, S. Ferber, and H. G. Weber, 160 Gbit/s 3R-regenerating wavelength converter, Proc. 7th Opto-Electronics and Communications Conference (OECC'02) at Yokohama, Japan, 2002, Post-deadline paper, PD1-3.

25. S. Watanabe, F. Futami, R. Okabe, Y. Takita, S. Ferber, R. Ludwig, C. Schubert, C. Schmidt, and H.G. Weber, 160 Gbit/s Optical 3R-Regenerator in A Fiber Transmission Experiment, Proc. Optical Fiber Communication Conference (OFC2003) at Atlanta, Georgia, USA, March 2003, Post-deadline Paper, PD16.

26. S. Watanabe, R. Ludwig, F. Futami, C. Schubert, S. Ferber, C. Boerner, C. Schmidt-Langhorst, J. Berger, and H.G. Weber, Ultrafast all-optical 3R-regeneration, IEICE Trans., **E87-C**, 1114–1118 (2004).

27. H. Takara, T. Ohara, K. Mori, K. Sato, E. Yamada, Y. Inoue, T. Shibata, M. Abe, T. Morioka, and K-I. Sato, More than 1000 channel optical frequency chain generation from single supercontinuum source with 12.5 GHz channel spacing, Electron. Lett., **36**, 2089–2090 (2000).

28. F. Futami, S. Watanabe, and T. Chikama, Simultaneous recovery of 20 × 20 GHz WDM optical clocks using supercontinuum in a nonlinear fiber: Proc. 26th European Conference on Optical Communication (ECOC2000) at Munich, Germany, September 2000, Post-deadline paper 2.8.

29. F. Futami and S. Watanabe, All-optical data addition to a time slot in 160-Gb/s OTDM signal using wavelength conversion by supercontinuum generation: Proc. 27th European Conference on Optical Communication (ECOC2001) at Amsterdam, Netherlands, September 2001, Paper WeB2, pp.306–307.

30. C. Schmidt, F. Futami, S. Watanabe, T. Yamamoto, C. Schubert, J. Berger, M. Kroh, H.-J. Ehrke, E. Dietrich, C. Boerner, R. Ludwig, and H.G. Weber, Optical Q-factor monitoring at 160 Gb/s using an optical sampling system in an 80 km transmission experiment, Proc. Conference on Lasers and Electro-Optics (CLEO 2002) at Long Beach, 2002, CThU3.

31. J. Li, J. Hansryd, P. O. Hedekvist, P. A. Andrekson, and S. N. Knudsen: 300 Gbit/s eye-diagram measurement by optical sampling using fiber based parametric amplification, Proc. Optical Fiber Communication Conference (OFC2001) at Anaheim, CA, 2001, Post-deadline paper.

32. N. Yamada, N. Banjo, H. Ohta, S. Nogiwa, and Y. Yanagisawa, 320-Gb/s eye diagram measurement by optical sampling system using a passively mode-locked fiber laser, Proc. Optical Fiber Communication Conference (OFC2002) at Anaheim, CA, 2002, Paper ThU3.

33. M. Shirane, Y. Hashimoto, H. Kurita, H. Yamada, and H. Yokoyama, Optical sampling measurement with all-optical clock recovery using mode-locked diode lasers, Proc. Optical Fiber Communication Conference (OFC2001) at Anaheim, CA, 2001, Paper MG2.

34. H. Takara, S. Kawanishi, A. Yokoo, S. Tomaru, T. Kitoh, and M. Saruwatari, 100 Gbit/s optical signal eye-diagram measurement with optical sampling using organic nonlinear optical crystal, Electron. Lett., **32**, 2256–2258 (1996).

35. K. Igawa, A. Otani, and Y. Tsuda, Novel Optical Sampling Oscilloscope without traditional trigger technique and measurement of optical short pulse modulated PRBS pattern, Proc. Optical Fiber Communication Conference (OFC 2004) at Los Angeles, 2004, CA, 2004, Paper MF73.

36. S. Watanabe, G. Ishikawa, T. Naito, and T. Chikama, Generation of optical phase-conjugate waves and compensation for pulse shape distortion in a single-mode fiber, J. Lightwave Technol., **12**, 2139–2146 (1994).

37. G. P. Agrawal, *Nonlinear Fiber Optics*, 2nd. ed. (Academic Press, San Francisco, CA, 1995).

38. K. Inoue, Four-wave mixing in an optical fiber in the zero-dispersion wavelength region, J. Lightwave Technol., **10**, 1553–1561 (1992).

39. M. Onishi, T. Okuno, T. Kashiwada, S. Ishikawa, N. Akasaka, and M. Nishimura, Highly nonlinear dispersion shifted fiber and its application to broadband wavelength converter, Proc. Integrated Optics and Optical Fiber Communications/24th European Conference on Optical Communications (IOOC/ECOC'97) at Edinburgh, UK, September 1997, Paper TU2C, pp.115–118.

40. C.D. Poole, and D.L. Favin: Polarization-mode dispersion measurements based on transmission spectra through a polarizer, J. Lightwave Technol., **12**, 917–929 (1994).

41. J.H.Lee, W. Belardi, K. Furusawa, P. Petropoulos, Z. Yusoff, T.M. Monro, D.J. Richardson, Four-wave mixing based 10-Gb/s tunable wavelength conversion using a holey fiber with a high SBS threshold, IEEE Photon. Technol. Lett., **15**, 440–442 (2003).

42. R. Hainberger, and S. Watanabe, Wavelength dependence of the nonlinear coefficient of highly nonlinear photonic crystal fibers, 9th Opto-Electronics and Communications Conference/3rd International Conference on Optical Internet (OECC/COIN2004) at Yokohama, Japan, July 2004, Paper 16E1-3.

43. P. Petropoulos, T.M. Monro, H. Ebendorff-Heidepriem, K. Frampton, R.C. Moore, H.N. Rutt, and D.J. Richardson, Soliton-self-frequency-shift effects and pulse compression in an anomalously dispersive high nonlinearity lead silicate holey fiber, Proc. Optical Fiber Communication Conference (OFC2003) at Atlanta, Georgia, USA, March 2003, Post-deadline paper PD3 Atlanta.

44. M. Asobe, H. Kobayashi, and H. Itoh, Laser-diode-driven ultrafast all-optical switching by using highly nonlinear chalcogenide glass fiber, Opt. Lett., **18**, 1056–1058 (1993).

45. N. Sugimoto, T. Nagashima, T. Hasegawa, S. Ohara, K. Taira, and K. Kikuchi, Bismuth-based optical fiber with nonlinear coefficient of 1360 $W^{-1}km^{-1}$, Proc. Optical Fiber Communication Conference (OFC 2004) at Los Angeles, 2004, CA, Post-deadline paper PD26.

46. S. Watanabe and M Shirasaki, Exact compensation for both chromatic dispersion and Kerr effect in a transmission fiber using optical phase conjugation, J. Lightwave Technol., **14**, 243–248 (1996).

47. A. Yariv, D. Fekete, and D.M. Pepper, Compensation for channel dispersion by nonlinear optical phase conjugation, Opt. Lett., **4**, 52–65 (1979).

48. S. Watanabe, T. Naito and T. Chikama, Compensation of chromatic dispersion in a single-mode fiber by optical phase conjugation, IEEE Photon. Technol. Lett., **5**, 92–95 (1993).

49. S. Watanabe, S. Kaneko, and T. Chikama, Long-haul fiber transmission using optical phase conjugation, Optical Fiber Technologies, **2**, 169–178 (1996).

50. T. Yamamoto, L.K. Oxenlowe, C. Schmidt, C. Schubert, E. Hilliger, U. Feiste, J. Berger, R. Ludwig, and H.G. Weber, Clock recovery from 160 Gbit/s data signals using phase-locked loop with interferometric optical switch based on semiconductor optical amplifier, Electron. Lett., **37**, 509–510 (2001).

51. O. Kamatani and S. Kawanishi, Prescaled timing extraction from 400 Gb/s optical signal using a phase lock loop based on four-wave-mixing in a laser diode amplifier, IEEE Photon. Technol. Lett., **8**, 1094–1096 (1996).

52. C. Boerner, S. Watanabe, F. Futami, R. Okabe, S. Ferber, C. Schubert, R. Ludwig, C. Schmidt-Langhorst, and H.G. Weber, 160 Gbit/s clock recovery in a 3R-regenerating wavelength converter, Proc. 30th European Conference on Optical Communication (ECOC2004) at Stochholm, Sweden, September 2004, Paper We3.5.6, pp. 440–441.

53. P.V. Mamyshev, All-optical data regeneration based on self-phase modulation effect, Proc. 24th European Conference on Optical Communications (ECOC'98) at Madrid, Spain, September 1998, 1, p. 475.

54. S. Watanabe, R. Okabe, F. Futami, R. Hainberger, C. Schmidt-Langhorst, C. Schubert, and H.G. Weber, Novel fiber Kerr-switch with parametric gain: Demonstration of optical demultiplexing and sampling up to 640 Gb/s, Proc. 30th European Conference on Optical Communication (ECOC2004) at Stockholm, Sweden, September 2004, Post-deadline paper Th4.1.6, pp.12–13.

55. J. Hansryd, P.A. Andrekson, M. Westlund, J. Li, P.-O. Hedekvist, Fiber-based optical parametric amplifiers and their applications, IEEE J. Select. Top. Quantum Electron., **8**, 506–520 (2002).

56. F. Futami, R. Okabe, Y. Takita, and S. Watanabe, Transparent wavelength conversion at up to 160 Gb/s by using supercontinuum generation in a nonlinear fiber, Proc. Optical Amplifiers and Applications (OAA 2003) at Otaru, Japan, 2003, Paper MD07.

57. S. Ferber, R. Ludwig, F. Futami, S. Watanabe, C. Boerner, C. Schmidt-Langhorst, L. Molle, K. Habel, M. Rohde, H.-G. Weber, 160 Gb/s regenerating conversion node, Proc. Optical Fiber Communication Conference (OFC2004) at Los Angeles, 2004, CA, 2004, Paper ThT2.

58. T. Akiyama, M. Ekawa, M. Sugawara, H. Sudo, K. Kawaguchi, A. Kuramatsu, H. Ebe, H. Imai, and Y. Arakawa, An ultrawide-band (120 nm) semiconductor optical amplifier having an extremely-high penalty-free output power of 23 dBm realized with quantum-dot active layers, Proc. Optical Fiber Communication Conference (OFC2004) at Los Angeles, 2004, CA, Post-deadline paper, PD12.